Reaction Chemistry & Engineering

ROYAL SOCIETY OF CHEMISTRY

PAPER

View Article Online
View Journal | View Issue

Check for updates

Cite this: *React. Chem. Eng.*, 2025, **10**, 561

A simple redox model of low-*T* NO + CO adsorption onto Pd-CHA as effective passive NOx adsorbers†

Umberto Iacobone, [a] Andrea Gjetja, [a] Nicola Usberti, [a] Isabella Nova, [a] Enrico Tronconi, *[a] Djamela Bounechada, [b] Roberta Villamaina, [b] Maria Pia Ruggeri, [b] Andrew P. E. York, [b] Loredana Mantarosie [b] and Jillian Collier [b]

Received 4th July 2024,
Accepted 15th November 2024

DOI: 10.1039/d4re00324a

rsc.li/reaction-engineering

Pd-exchanged chabazite (Pd-CHA) catalysts show NO adsorption and desorption features which comply well with the requirements for low-*T* passive NOx adsorber (PNA) applications. An earlier work based on transient adsorption tests investigated the NO storage pathway on Pd-CHA, a still debated topic in the literature. Such research highlighted a Pd-redox mechanism ($Pd^{2+} \leftrightarrow Pd^{+}$) underlying the NO storage chemistry over these systems. CO and NO were capable of reducing Pd^{2+} at low temperatures, and the newly formed Pd^{+} acted as the main NO storage site. Increasing temperatures activated a Pd-oxidation process, which reduced the fraction of Pd^{+} sites, and consequently the NO storage, but was inhibited by H_2O. Herein we challenge quantitatively such a scheme relying on transient kinetic analysis. We show that a simple redox kinetic model of NO + CO storage on Pd-CHA, based on the above, reproduces the main features of the species evolution and of the NO storage observed under variable operating conditions over Pd-CHA samples with two Pd-loadings, thus lending support to the proposed Pd-redox chemistry.

1. Introduction

The mitigation of NOx emissions from diesel-fuelled vehicles under cold-start conditions is still a prominent challenge in the environmental sector. The progressive enhancements of modern internal combustion engines have increased their fuel-efficiency, however lowering the exhaust gas temperatures. This aspect has worsened the deNOx performance of the current state-of-the-art aftertreatment technologies, such as lean NOx traps (LNT) and NH_3-selective catalytic reduction (NH_3-SCR) since their respective catalysts are characterized by light-off temperatures typically above 200 °C.[1–4] Thus, extended warm-up phases are required by the catalytic converters to reach an appropriate thermal regime for pollutant abatement. This presents the cold-start period as the main source of NOx during vehicular operation.[5] To cope with the increasing tightening of environmental regulations, a promising option is the adoption of systems such as passive NOx adsorbers (PNAs), upstream with respect to the main catalytic converter. These systems are designed to trap the low-temperature NOx (low-*T*, <200 °C), in particular NO, for later thermal release once the downstream reduction catalysts become active.[6–12] Among several catalysts tested as potential PNA materials, Pd-exchanged small-pore zeolites (Pd-CHA) have emerged as the catalyst of choice. The remarkable capacity to adsorb low-*T* NOx, mainly as NO, an appropriate desorption temperature window, the resistance to sulphur and hydrocarbon poisoning, and the good hydrothermal stability make Pd-CHA an ideal material for these applications in comparison to other formulations (*e.g.*, ceria/alumina-supported Pd/Pt, Pd-BEA).[9,10,13–18] Nevertheless, despite extensive investigation, no consensus has been reached yet on the NOx adsorption/desorption pathways for such systems and the nature of the associated active sites.

Several works have reported the existence of a variety of Pd sites for NO adsorption, in the form of clusters, nanoparticles, and metal-exchanged sites, supported by experimental and theoretical findings.[6,7,9,13,14,19–23] Among these, isolated Pd cations are recently emerging as prominent and effective low temperature NO adsorption sites.[9,14,20,24,25]

Combined experimental evidence from kinetic studies, DFT computational work, XPS, EXAFS, DRIFT, and FT-IR spectroscopy suggests the role of Pd^{2+} and Pd^{+}, acting as the NO storage centres, forming nitrosyl complexes, following both adsorption pathways and a Pd-redox chemistry where NO reduces Pd^{2+} to Pd^{+}, releasing NO_2.[9,13,14,20,24–30] The

[a] *Laboratory of Catalysis and Catalytic Processes, Dipartimento di Energia, Politecnico di Milano - Via La Masa, 34, 20156 Milano, Italy. E-mail: enrico.tronconi@polimi.it; Tel: +39 02 23993264*
[b] *Johnson Matthey Technology Centre - Blounts Court Road, Sonning Common, Reading RG4 9NH, UK*

† Electronic supplementary information (ESI) available. See DOI: https://doi.org/10.1039/d4re00324a

identification of the primary storage site remains, however, controversial, as some suggest Pd^+ (ref. 22, 23 and 26–28) while others support oxidized Pd species.[13,31] Furthermore, it has been acknowledged that the nature of the Pd species can change also according to the catalyst features (silica–alumina ratio, Pd loading, zeolite framework), the pre-treatment, the reaction conditions, and the zeolite synthesis method.[11,13,25,26,29,32,33] Similarly to NO, also CO has been proposed as a Pd reducing agent, enhancing the system storage due to its stronger interaction with Pd, and releasing CO_2 as a result.[26] A negative impact of water in the NO storage over different Pd-exchanged zeolites has been observed, supported by theoretical calculations, which demonstrated the lowering of the NO binding energies with Pd in its presence.[9,13,14,31]

Kinetic studies were conducted to elucidate the features of transient NO uptake and desorption over Pd-promoted zeolites, following complex reaction pathways. In the works of Ambast *et al.*[27,34] and Yao *et al.*,[21] PNA monolith materials were tested, and satisfactory kinetic descriptions were obtained considering reaction mechanisms with multiple-steps (9 and 10, respectively) for NO-only feed, with 9 additional steps in the presence of CO. Several adsorption phases, with the intermediate formation of surface complexes, and two-step Pd^{2+} reductions, releasing NO_2 or CO_2, were proposed. Ambast *et al.*[27,34] accounted for Pd cations-only as active NO storage sites (*i.e.* Z-$[Pd^{2+}OH]^+$, Z_2Pd^{2+}, and ZPd^+), while Yao *et al.*[21] included also PdO as an additional adsorption centre. Furthermore, CO was proposed to further reduce Pd^+ and PdO to Pd^0 and metallic Pd respectively.[21]

In this context, in a previous study we reported NO adsorption chemistry over a Pd-CHA sample, relying on transient adsorption experiments at variable operative conditions.[35] The simple integral analysis of the gas phase transients permitted the interrogation of the underlying NO storage mechanism, which clearly followed a Pd-redox chemistry. The majority of palladium existed initially as Pd^{2+}, which was readily reduced to Pd^+ by CO, or NO, acting as reducing agents. The study highlighted a more favourable NO storage under reducing conditions, *i.e.* on Pd^+, while the activation of Pd-oxidation processes, converting Pd^+ back to Pd^{2+}, decreased the available NO adsorption sites thus leading to a decrement in the overall NO storage.[23,35] Interestingly, the presence of water apparently inhibited Pd-oxidation, resulting in a positive effect on NO storage which was not observed previously in the literature. These findings were recently supported by an independent DFT investigation.[23]

With the intent to challenge quantitatively the NO adsorption chemistry proposed in previous work,[35] a transient kinetic redox model has been herein developed and applied to describe the NO adsorption pathway. To strengthen the analysis, the model has been fitted to transient data covering three different gas phase compositions (effects of NO, CO, and H_2O) over four adsorption temperatures in the low-T range (100–200 °C) and collected over two catalysts characterized by different Pd-loadings. Notably, the proposed kinetic model simplifies those already reported in the literature,[21,27,34] relying on fewer reaction steps and fewer intermediate complexes, while further showcasing the central role of the Pd-redox chemistry in the NO storage mechanism.

2. Materials and methods

2.1 Catalyst samples and experimental set-up

Two Pd-CHA catalysts in the form of powder, both supplied by Johnson Matthey, have been considered in this study. The reference material was characterized in a previous work by ICP-MS analysis, resulting in a Pd loading of 0.84% w/w and SiO_2/Al_2O_3 (SAR) of 25.[35] To study the impact of the Pd-loading on the PNA functionality, a second sample with Pd-content and SAR respectively of 0.50% w/w and 25 have been herein investigated, too. Throughout the manuscript, the two catalysts are labelled as 0.84% Pd and 0.50% Pd. A lean hydrothermal aging procedure (LHA) at 750 °C for 16 h in air with 10% H_2O ensured the proper Pd particle redispersion forming exchanged ions, with negligible PdOx clusters, as shown by UV-vis and EXAFS analysis on both the 0.84% Pd and 0.5% Pd catalysts.[35] This is also proven by the equimolar NO adsorption in respect to the Pd detected by ICP-MS (NO : Pd = 1 : 1) in NO + O_2 wet tests at low temperature.[35]

Two tubular quartz micro-flow reactors were prepared (ID ≈ 6 mm), one per catalyst, each loaded with 130 mg of powder mixture (40 mg of catalyst + cordierite diluent). A thermocouple inserted in the catalyst bed was used to measure the reactor temperature. The samples were tested in an experimental set-up where helium was used as gas mixture dilutant. The reactants (NO, CO, O_2) were dosed with mass flow controllers (Brooks Instruments) and traced with Argon, while the water vapor feed concentration was regulated with an electrically heated saturator. A combination of a UV analyser (ABB LIMAS 11 HW) + IR analyser (ABB URAS 14) with a mass spectrometer (QGA Hiden Analytical) enabled to monitor the reactor outlet composition (NO, NO_2, CO, CO_2, O_2, H_2O, Ar). Additional information on the experimental set-up and protocols can be found in previous publications.[35–37]

2.2 Transient adsorption/desorption protocol

The transient adsorption/desorption procedure to evaluate the Pd-CHA functionality as PNA materials, with variable gas phase composition and adsorption temperature, was described previously.[35]

A constant GHSV of 300 000 $cm^3\ h^{-1}\ g_{cat}^{-1}$ (STP) has been adopted in the tests herein presented. Prior to each experiment, a high temperature treatment with 10% v/v of O_2 at 500 °C was performed to remove previously adsorbed species and fully oxidize the palladium.[35] A cooling phase in the same oxidizing atmosphere followed. If required, H_2O was added to the feed when close to the test operative

temperature. An initial 50 min isothermal adsorption phase was carried out in the presence of different feed gas mixtures ($NO + O_2$ dry-gas, $NO + O_2$ wet, $CO + NO + O_2$ dry-gas; NO = 0–200 ppm, CO = 0–1500 ppm, O_2 = 10% v/v, H_2O = 0–5% v/v) and temperatures (100, 120, 150, 200 °C). Additionally, dedicated tests with the $CO + NO + O_2$ feed mixture, where the NO step feed was delayed with respect to CO, were performed (called "$CO + O_2$ + delayed NO" in the following). Initially applied on the 0.84% Pd sample, these protocols have been replicated on 0.50% Pd as well, limited to the adsorption temperature of 100 °C.[35]

It is well known that, at low temperatures, CO can reduce Pd to its metallic form, originating sintering phenomena: accordingly, we avoided to work at temperatures below 100 °C. In addition, all the tests, both with NO and with CO, have been run in the constant presence of 10% v/v of oxygen. In our experience, this further reduces the chances of fully reducing the palladium sites. To prove that no deactivation occurred throughout different tests in these conditions, Fig. SI.1† shows a sequence of $NO + O_2$ temperature programmed surface reaction (TPSR) runs in a wet atmosphere: each run was executed after a $CO + O_2$ test and no significant difference between them is apparent, indicating that the Pd sites were not considerably altered by repeated exposure to CO.

2.3 NO adsorption kinetic model

As discussed in the Introduction, the NO adsorption mechanism on Pd-CHA remains debated, with different pathways proposed in the literature.[6,7,9,13,14,19–21] In the present work, we mainly rely on the mechanistic investigation of NO trapping performed previously over the 0.84% Pd.[23,35] The goal of this work is to create a simple but chemically based kinetic mechanism which can accurately represent the behaviour of the PNA system in the low-temperature regime and use it to validate our mechanistic understanding with a minimum set of reaction steps. For this purpose, while a large variety of reactions has been considered in literature, several of them were ruled out in this work. An example of ruled-out reactions is the thermal desorption of NO or CO: in fact, these reactions are not relevant for the present kinetic analysis due to their very poor activity in the low-temperature regime, as addressed here.[35] Consistently with these considerations, the assumed reaction steps are summarized in Table 1.

Analysis of flow reactor experiments led to the proposal of a Pd-redox NO adsorption chemistry, wherein Pd cycles between Pd^{2+} and Pd^{+}, involving a strong link between the Pd reduction extent and the NO storage capacity.[23,35] As discussed in the Introduction, the role of a redox chemistry in Pd-CHA systems has been proposed in several works. However, herein we regard it as the main pathway leading to stable NO adsorption.[9,13,14,20,24–30] CO primarily, and NO to a lesser extent, act as Pd^{2+} reductants according to a dual-site catalytic chemistry producing CO_2 or NO_2 respectively ((R1) and (R5)).[14,23,26,27,34,38]

The key role of $ZPd^{2+}OH$ in such a mechanism has already been reported, even though the Pd^{2+} population may include also other species, like the doubly ligated Z_2Pd^{2+}.[13,14,23,31] In fact, it is generally accepted that Z_2Pd^{2+} species are not prone to be reduced, contrary to the redox-active $ZPd^{2+}OH$.[27] In our tests we were able to fully reduce the Pd catalyst with dry CO + O_2 already at 100 °C, producing CO_2.[35] Thus, even if our oxidized Pd-CHA samples may not contain exclusively ZPd^{2+}-OH in their pristine state, all the Pd^{2+} cations need eventually to be converted to such species in order to be reduced and then adsorb CO. Considering that H_2O molecules are available on the zeolite, a possible explanation is provided by the hydrolysis reaction $Z_2Pd^{2+} + H_2O \rightleftharpoons ZPd^{2+}OH + ZH^{+}$, whose equilibrium is shifted towards the monodentate ZPd^{2+}-OH form by its consecutive reactivity with CO (a so-called scavenging reaction). This is similar to the Z_2Cu^{2+} hydrolysis documented over Cu-CHA catalysts for NH_3-SCR.[39]

In a recent FTIR *in operando* study of CO adsorption on Pd-CHA, Lietti and co-workers[40] have reported that, at room temperature and under dry-gas conditions, CO was adsorbed onto Z_2Pd^{2+} sites. When water was added to the gas feed,

Table 1 Simple redox kinetic mechanism for CO and NO adsorption onto Pd

Reaction no.	Reaction step	Reaction rate expression [s^{-1}]
(R1)	$2Pd^{2+}OH + CO \rightarrow 2Pd^{+} + CO_2 + H_2O$	$r_1 = k_1 \frac{y_{CO}}{500} \sigma^2_{Pd^{2+}OH}$
(R2)	$Pd^{+} + CO \rightarrow Pd^{+}CO$	$r_2 = k_2 \frac{y_{CO}}{500} \sigma_{Pd^{+}}$
(R3)	$Pd^{+}CO + NO \rightarrow Pd^{+}NO + CO$	$r_3 = k_3 \frac{y_{NO}}{500} \sigma_{Pd^{+}CO}$
(R4)	$Pd^{2+}OH + NO \rightleftharpoons Pd^{2+}OH(NO)$	$r_4^{ads} = k_4^{ads} \frac{y_{NO}}{500} \sigma_{Pd^{2+}OH}$ $r_4^{des} = k_4^{des} \sigma_{Pd^{2+}OH(NO)}$
(R5)	$2Pd^{2+}OH(NO) + NO \rightarrow 2Pd^{+}NO + NO_2 + H_2O$	$r_5 = k_5 \frac{y_{NO}}{500} \sigma^2_{Pd^{2+}OH(NO)}$
(R6)	$2Pd^{+}NO + \frac{1}{2}O_2 + H_2O \rightarrow 2Pd^{2+}OH + 2NO$	$r_6 = k_6 \sqrt{\frac{y_{O_2}}{500}} \sigma^2_{Pd^{+}NO}$
(R7)	$2Pd^{+}CO + \frac{1}{2}O_2 + H_2O \rightarrow 2Pd^{2+}OH + 2CO$	$r_7 = k_7 \sqrt{\frac{y_{O_2}}{500}} \sigma^2_{Pd^{+}CO}$

though, a complete shift of the IR bands towards the region of Pd(I) carbonyls proved the hydrolysis of the Z_2Pd^{2+} sites to $ZPd^{2+}OH$, which are readily reducible and enabled adsorption of CO in a stable form as Pd^{+}–CO. This picture is fully consistent with our CO storage mechanism, steps (R1) and (R2) in Table 1, and supports the assumption of $ZPd^{2+}OH$ as the dominant oxidized Pd species, as well as the precursor of the primary storage site for NO and CO, *i.e.*, Pd^{+}, in our simple redox model.

While the evidence for the conversion of Z_2Pd^{2+} sites to $ZPd^{2+}OH$ under wet conditions (*i.e.*, with H_2O in the feed stream) experiments are solid,[40] this is less clear for our experiments under dry-gas conditions (*i.e.*, with no H_2O added to the feed stream). Indeed, in our protocols the catalysts are pre-heated to 500 °C also to dehydrate the powder samples. However, we speculate that this pretreatment did not remove all the moist in the small-pores zeolite cages of our Pd-CHA systems, so that the residual H_2O could still promote the hydrolysis step. Accordingly, we retain the assumption of the Pd^{2+} population consisting primarily of $ZPd^{2+}OH$ for dry-gas conditions, too.

The proposal of two $ZPd^{2+}OH$ species involved in (R1) and (R5) originated from a quantitative analysis of the reacting system: throughout the different NO adsorption tests, a maximum 1 : 2 molar ratio between CO_2, or NO_2, release and the overall Pd content was noted under both wet and dry-gas conditions, consistent with the involvement of an O-donor species and with the two-electron exchange requirements of (R1) and (R5), where the Pd^{2+} reduction to Pd^{+} needs one electron transfer per Pd. Notably, the results from the CO oxidation tests indicate that two $Pd^{2+}OH$ cations are always available in close proximity, both under dry-gas and wet conditions.[35] This suggests that the Pd sites are mobile, possibly because H_2O-solvated. While this is reasonable for wet experiments,[40] in the case of dry-gas experiments we have again to assume, similar to the previous considerations on the Z_2Pd^{2+} hydrolysis, that residual H_2O in the zeolite can confer enough mobility to the Pd sites to enable the CO oxidation activity we have observed also in dry-gas conditions.

The detailed analysis of the Pd-speciation is outside the scope of this work: it must be mentioned, however, that the same considerations above may be consistent also with the involvement of Pd dimers (*e.g.*, $[Pd–O–Pd]^{2+}$).[13,14,23,31] In fact, for the CO to CO_2 oxidation reaction (R1), similar conclusions were drawn by several studies conducted previously using CO as a probe molecule to assess the presence of binuclear Cu^{2+} species, originating from the coupling of mobile $Cu^{2+}OH$ ions, over Cu-CHA catalysts for NH_3-SCR applications.[36,39,41,42]

Once reduced, Pd^{+} acts as the main NO adsorption site,[23,26–28] forming $Pd^{+}NO$; adsorption of CO is also possible (R2), however when NO is present CO is displaced from Pd^{+}, and the competitive NO adsorption is favoured (R3).[29,35] In addition to this primary NO storage mechanism, a weak reversible NO storage on the oxidized Pd^{2+} is also accounted for by reaction (R4), mainly active when CO is not present.[23,26] The palladium utilization factor (*i.e.*, adsorbed NO/Pd molar ratio) was shown to be a decreasing function of temperature.[35] Indeed, an increasing temperature progressively activates Pd^{+} oxidation: Pd^{+} is converted back to $Pd^{2+}OH$, thus leading to a decrease in the number of available NO and CO adsorption sites. This process is herein accounted for by (R6) and (R7) in Table 1.[21] Globally, five Pd-species are included in the considered adsorption scheme: two oxidized palladium species – $Pd^{2+}OH$ and $Pd^{2+}OH(NO)$ – and three reduced species – Pd^{+}, $Pd^{+}CO$ and $Pd^{+}NO$.

Remarkably, the adsorption of NO onto Brønsted Acid Sites (BAS) has been disregarded. Indeed, previous work on the proton form of the CHA zeolite demonstrated that, in dry-gas conditions, only minor amounts of NO were weakly adsorbed, which were readily desorbed isothermally in helium, while under wet conditions NO adsorption was not observed at all.[35]

The kinetic analysis of the transient NO adsorption steps for the 0.50% Pd and 0.84% Pd samples relies on the abovementioned reaction mechanism. Table 1, 3rd column, lists the turnover rate expressions of the k-reactions (r_k) adopted for the reaction steps ((R1) to (R7)), where k_k are apparent rate constants. These equations assume first-order reaction kinetics in the gaseous species (NO, CO), with the NO and CO concentrations normalized by a reference feed concentration (500 ppm). Conversely, a second-order dependence on the oxidized and reduced Pd fractions, respectively, has been postulated for the two-electron exchange Pd reduction and re-oxidation steps ((R1) and (R5)–(R7)). While alternative first-order dependences would result in a similar goodness of fit, the adopted second-order assumption is in line with the recent literature on kinetic modelling of PNA systems, see *e.g.* the dual-site steps in the models published by Olsson and coworkers[21] and by Harold and coworkers.[27]

To estimate the associated rate parameters, the transient gas phase species evolution was fitted adopting a transient integral plug-flow model of the test reactor, modelled as a cascade of 20 isothermal, isobaric continuous stirred tank reactors (CSTR). A similar approach has been successfully utilized in the kinetic analysis of transient NH_3-SCR experiments over Cu-CHA catalysts.[37,43,44] The mass balance equations for the gaseous species and for the Pd sites in each CSTR are reported in Tables 2 and 3, respectively.

For each i-gas species, y^{in} and y are respectively the inlet and outlet molar fractions in each CSTR, τ_R is the residence time in each CSTR and τ_{cat} is the contact time, evaluated as n_{Pd}/F [mol_{Pd} mol^{-1} s^{-1}], where n_{Pd} is the Pd loading in each CSTR and F is the molar feed flow. σ_j is the molar fraction of a Pd j-species in each CSTR, as n_j/n_{Pd} [mol_{Pd_j} mol_{Pd}^{-1}] and n_{Pd} is the respective molar content.

A code written in FORTRAN language has been used for numerical integration of the PDE system in time for each CSTR reactor. For this purpose, we used the SLSODE solver for ordinary differential equations (ODEs),

Table 2 Gas phase CSTR model equations for the NO adsorption reaction scheme

Equation no.	Gaseous species	Gas phase mass balance [–]
(1)	NO	$\tau_R \frac{\partial y_{NO}}{\partial t} = y_{NO}^{in} - y_{NO} + \tau_{cat}(-r_3 - r_4^{ads} + r_4^{des} - r_5 + 2r_6)$
(2)	CO	$\tau_R \frac{\partial y_{CO}}{\partial t} = y_{CO}^{in} - y_{CO} + \tau_{cat}(-r_1 - r_2 + r_3 + 2r_7)$
(3)	NO_2	$\tau_R \frac{\partial y_{NO_2}}{\partial t} = y_{NO_2}^{in} - y_{NO_2} + \tau_{cat} r_5$
(4)	CO_2	$\tau_R \frac{\partial y_{CO_2}}{\partial t} = y_{CO_2}^{in} - y_{CO_2} + \tau_{cat} r_1$

Table 3 Pd species and kinetic CSTR model equations for the NO adsorption reaction scheme

Equation no.	Pd-species	Pd-species mass balance [$mol_{Pd_j}\ mol_{Pd_{tot}}^{-1}\ s^{-1}$]
(5)	$Pd^{2+}OH$	$\frac{\partial \sigma_{Pd^{2+}OH}}{\partial t} = -2r_1 - r_4^{ads} + r_4^{des} + 2r_6 + 2r_7$
(6)	$Pd^{+}NO$	$\frac{\partial \sigma_{Pd^{+}NO}}{\partial t} = r_3 + 2r_5 - 2r_6$
(7)	Pd^{+}	$\frac{\partial \sigma_{Pd^{+}}}{\partial t} = 2r_1 - r_2$
(8)	$Pd^{+}CO$	$\frac{\partial \sigma_{Pd^{+}CO}}{\partial t} = r_2 - r_3 - 2r_7$
(9)	$Pd^{2+}OH(NO)$	$\sigma_{Pd^{2+}OH(NO)} = 1 - \sigma_{Pd^{2+}OH} - \sigma_{Pd^{+}NO} - \sigma_{Pd^{+}} - \sigma_{Pd^{+}CO}$

originally proposed for initial-value problems with stiff and non-stiff systems of first order ODEs by Hindmarsh,[45] and successfully implemented in earlier works.[37,43]

To validate the NO adsorption chemistry proposed in this work, a simple kinetic modelling approach has been implemented. Individual portions of the low-T redox model were fitted independently to dedicated sets of experimental data. Thus, k_1 and k_2 were estimated by adapting the model to the CO and CO_2 transients of the CO + O_2 + delayed NO experiment (first part, in absence of NO). Subsequently, k_3 was calibrated to account for the NO transients and the CO release with the delayed NO feed. The CO + O_2 + delayed NO test was also used to extract an estimate of k_7 from the steady-state production of CO_2 both in the first and in the second part of the run. Additionally, the NO + O_2 tests were used to estimate k_4–k_6 independently, fitting the NO and NO_2 profiles for k_4, the NO_2 peak for k_5 and the steady-state production of NO_2 for k_6 together with the fit of the NO + O_2 TPSR. Then, the co-feed of CO and NO, the water effect in the presence of only NO, the adsorption temperature effect, and the Pd-loading impact have all been predictively simulated just relying on the previously estimated rate parameters.

The goal of studying the PNA kinetics in absence and in presence of water is to elucidate the effect of H_2O on the different reaction steps, primarily to validate quantitatively our mechanistic understanding, rather than deriving empirical kinetic dependences on H_2O, which is out of scope and would require a dedicated set of experiments at different H_2O feed concentration.

3. Experimental results and kinetic modelling

The transient NO and/or CO adsorption and desorption tests are performed following the experimental protocols described in Materials and methods section, varying the gas phase feed composition, the Pd content, and the adsorption temperature. While the experimental results over the 0.84% Pd sample have been reported in our previous work,[35] herein we focus on the kinetic modelling of the isothermal

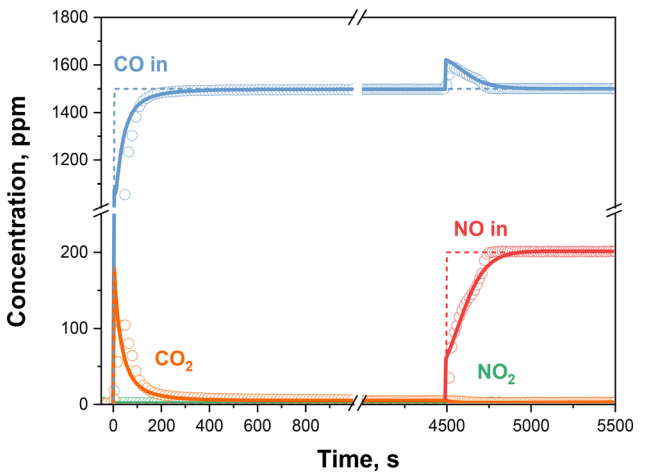

Fig. 1 CO + O_2 + delayed NO feed mixture: nominal inlet concentrations (dashed lines), experimental results (dots) and kinetic fit (solid lines) over 0.84% Pd sample. T = 100 °C, W_{cat} = 40 mg, GHSV = 300 000 $cm^3\ h^{-1}\ g_{cat}^{-1}$ (STP). Gas feed: NO = 0–200 ppm, CO = 1500 ppm, O_2 = 10% v/v, H_2O = 0% v/v.

adsorption step. The complete list of the estimated apparent rate constants is provided in Tables SI.1 and SI.2 of the ESI.†

3.1 Gas mixture composition effect

We start by discussing the kinetic analysis of the NO adsorption step with different feed gas mixtures at 100 °C over the 0.84% Pd sample. Fig. 1 shows the experimental data (dots) in the presence of a CO + O_2 + delayed NO feed mixture.

Upon feeding CO, a CO_2 production is readily observed, characterized by an initial peak and a monotonic decreasing trend until reaching an almost null steady state value.[35] The involvement of oxygen in the system chemistry can be ruled out, and the CO_2 formation is thus ascribed to the $Pd^{2+}OH$ reduction by CO according to the dual site CO oxidation step (R1) in Table 1. Concurrently, CO is weakly adsorbed on the reduced Pd^{+} and the $Pd^{+}CO$ could be oxidized back by oxygen according to reactions (R2) and (R7), respectively. The bonding of NO with Pd^{+} sites is however favoured with respect to CO, resulting in a displacement of CO upon NO feed, as described by reaction (R3).[29,35] The quantitative analysis of such experiments has been reported earlier; it highlighted: i) the complete reduction of Pd^{2+} to Pd^{+} by CO, ii) an equimolar displacement between the desorbed CO and the stored NO, iii) a complete Pd utilization, as confirmed by the NO/Pd molar ratio in Fig. 2.[35] Consistent with the proposed reaction scheme, no release of NO_2 is observed during the NO feed, since the NO_2 formation step (R5) requires the presence of $Pd^{2+}OH$, which was already reduced by CO during the initial step feed. Thus, no further reactions are considered here.

Such an experimental protocol enables to estimate the apparent rate constants of (R1), (R2), and (R7) (k_1, k_2 and k_7) independently from (R3) (k_3). The result of the kinetic fit is shown in Fig. 1 (continuous lines), where an accurate description of all the gas species transients is apparent. Indeed, both the CO and CO_2 features are faithfully reproduced during the CO-only feed. The same fit quality is observed for the displacement phenomena caused by the NO step feed. Furthermore, the model successfully predicts the integral NO storage, as plotted in Fig. 2. The Pd utilization factor (NO/Pd) is evaluated extrapolating the model to very long times, corresponding to fully developed steady-state profiles.

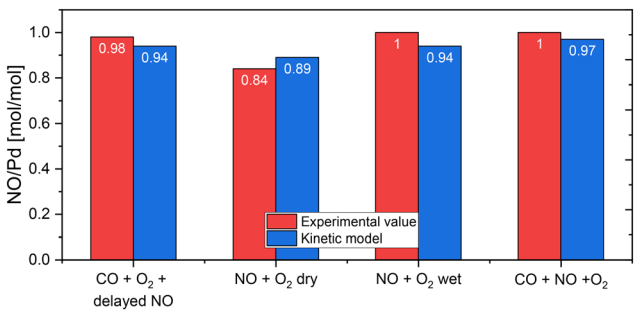

Fig. 2 Comparison between the experimental NO storage efficiency (red bars) and the model estimate (blue bars), with different gas phase compositions, on the 0.84% Pd sample at 100 °C.

The kinetic analysis of the NO + O_2 system, in the absence of CO, enable effective estimation of the apparent rate constants of reactions (R4) to (R6) (k_4 to k_6), independently from the previously described CO-related phenomena. Fig. 3 displays the experimental data, in dry-gas (A) and wet (B) conditions.

In close correspondence to the previous CO-step feed, a release of NO_2 is detected once NO is stepwise introduced in the feed stream. However, unlike CO_2, the rate of release of NO_2 is slow, despite the fast NO adsorption. Thus, a reversible adsorption on the oxidized $Pd^{2+}OH$ is proposed (R4), forming the $Pd^{2+}OH(NO)$ species.[23,26,38] Subsequently, NO interacts with such complexes being oxidized to NO_2 (R5), thus reducing two Pd species similarly to the CO pathway (R1). In the absence of water (Fig. 3A), an incomplete Pd oxidation is observed. Since NO is a weaker Pd reductant than CO, this experiment is likely affected by Pd-reoxidation phenomena (R6) even at low temperatures, resulting in an incomplete NO storage efficiency (NO/Pd = 0.84, as shown in Fig. 2).[35] Conversely, when cofeeding water (Fig. 3B), complete NO storage is recovered (NO/Pd = 1.00). This positive effect is rationalized by an inhibition effect of H_2O on the Pd-oxidation reaction (R6), which otherwise hinders the NO reduction extent of Pd^{2+}.[35]

The kinetic model successfully fits the transient species evolutions in the case of the NO + O_2 mixture, with and without water added to the feed, as shown in Fig. 3A and B (solid lines). The apparent rate constants (k_4 to k_6), are estimated from the first case only, while the water effect has been simulated by simply deactivating the Pd-oxidation reaction (R6). However, the very few ppm of NO_2 in the NO + O_2 dry-gas experiment do not enable a reliable estimation of the rate constant for (R6). Thus, k_6 has been estimated by fitting the TPSR run in the NO + O_2 dry-gas atmosphere shown in Fig. 4 (brown dots). This test follows the one shown in Fig. 3A, and shows how NOx are desorbed when the temperature is raised up to 500 °C with a ramp of 15 °C min^{-1}. To fit the TPSR profile, an Arrhenius form of the rate constant is needed $\left(k = k_0 \exp\left(-\frac{E_A}{RT}\right)\right)$, where the two parameters to be fitted are k_0 and E_A. The brown solid line Fig. 4 shows the model fit of the TPSR curve, which is in close agreement with the experimental trace. The model is also able with good accuracy to follow the NO and NO_2 dynamics over temperature during the T-ramp, as in Fig. SI.2.†

Finally, once we combine both k_4 and k_5 estimated from the adsorption test with k_6 estimated from the desorption step, the predicted NO storage capacity, albeit with some minor over/under-estimations, closely matches the experimental one for both the NO + O_2 dry-gas and wet tests (Fig. 2), so that the simple approach in the simulation

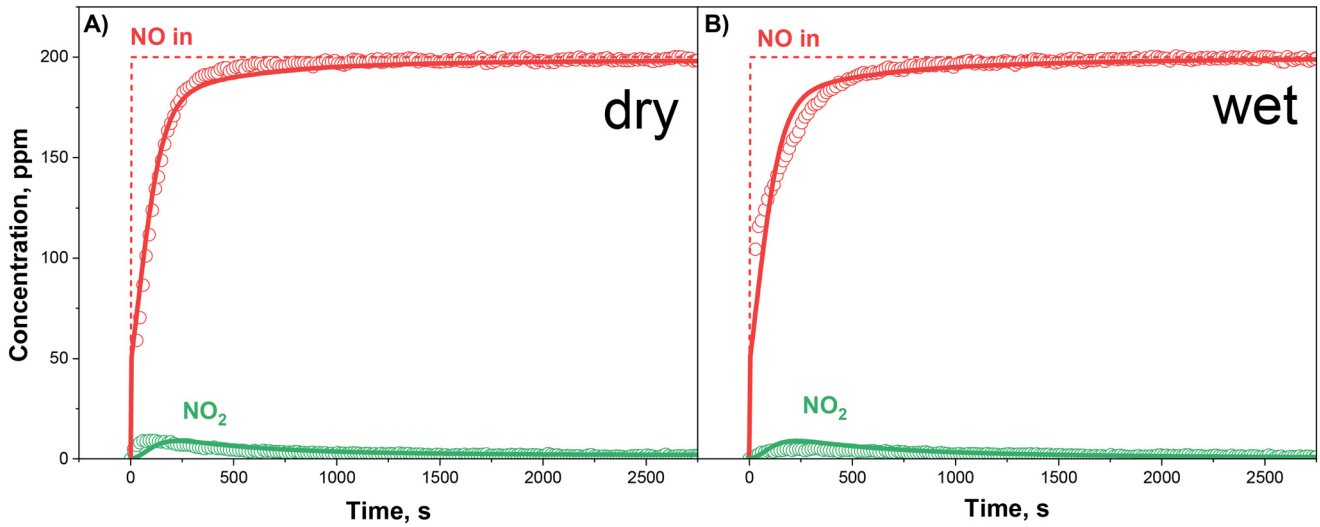

Fig. 3 NO + O_2 step feed on the 0.84% Pd sample, under dry-gas (A) and wet (B) conditions: nominal inlet concentrations (dashed lines), experimental results (dots), kinetic fit (solid lines, A) and kinetic simulation (solid lines, B). T = 100 °C, W_{cat} = 40 mg, GHSV = 300 000 $cm^3\ h^{-1}\ g_{cat}^{-1}$ (STP). Gas feed: NO = 200 ppm, CO = 0 ppm, O_2 = 10% v/v, H_2O = 0–5% v/v.

of the H_2O impact (turning off the (R6)) appears to be effective.

Lastly, the case with the co-feed of NO and CO is considered, with the experimental species evolutions shown in Fig. 5. The system features resemble closely those observed in the delayed feed case (Fig. 1), namely CO_2 production followed by CO displacement in correspondence to the NO adsorption, with similar considerations related to the quantitative analysis.[35]

The solid lines in Fig. 5 represent the model simulation based on the apparent rate constants previously estimated from the CO + O_2 + delayed NO (k_1, k_2, k_3 and k_7) and NO + O_2 (k_4, k_5 and k_6) runs. A satisfactory prediction of the evolution of both species and of the NO integral storage (as shown in Fig. 2) is apparent, validating the model based on a simple Pd-redox scheme where CO acts as the main reducing species, according to a dual-site mechanism over $Pd^{2+}OH$, and where Pd^+ is the main adsorption site. Furthermore, the negligible NO_2 production expected according to the considered kinetic model, once CO is present, is also found in agreement with the experimental results.

3.2 Pd-loading effect

A duplicate set of experiments with the NO + O_2 dry-gas, NO + O_2 wet and CO + NO + O_2 dry-gas feed mixtures has been

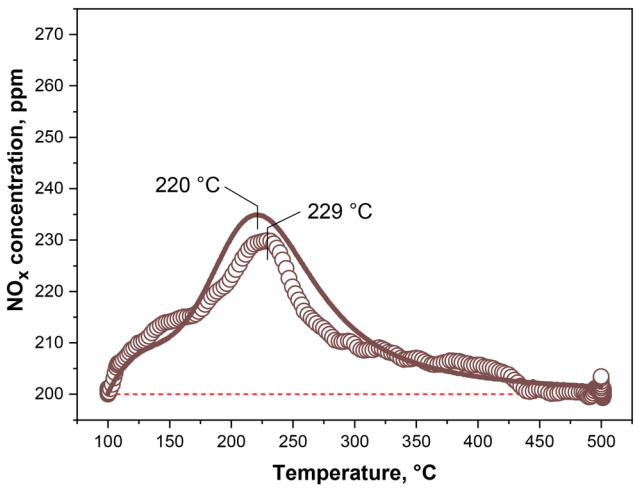

Fig. 4 Temperature programmed surface reaction (TPSR) test in a NO + O_2 dry-gas atmosphere on the 0.84% Pd-CHA sample: NO feed concentration (dashed line), experimental NOx trace (dots), kinetic fit (solid lines). T = 100–500 °C at 15 °C min^{-1}, W_{cat} = 40 mg, GHSV = 300 000 $cm^3\ h^{-1}\ g_{cat}^{-1}$ (STP). Feed: NO = 200 ppm, CO = 0 ppm, O_2 = 10% v/v, H_2O = 0% v/v.

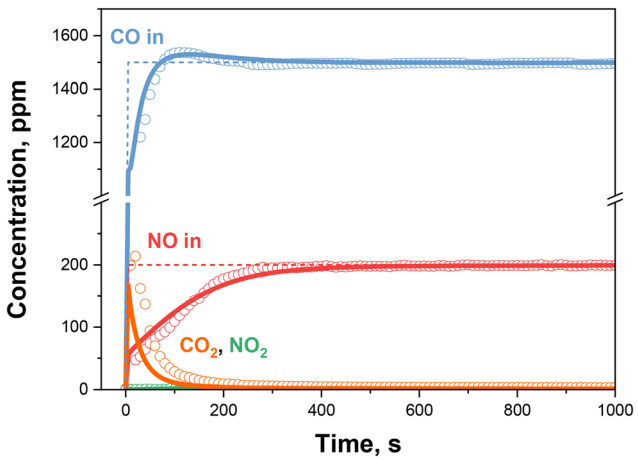

Fig. 5 CO + NO + O_2 step feed: nominal inlet concentrations (dashed lines), experimental results (dots) and kinetic simulations (solid lines) over the 0.84% Pd sample. T = 100 °C, W_{cat} = 40 mg, GHSV = 300 000 $cm^3\ h^{-1}\ g_{cat}^{-1}$ (STP). Gas feed: NO = 200 ppm, CO = 1500 ppm, O_2 = 10% v/v, H_2O = 0% v/v.

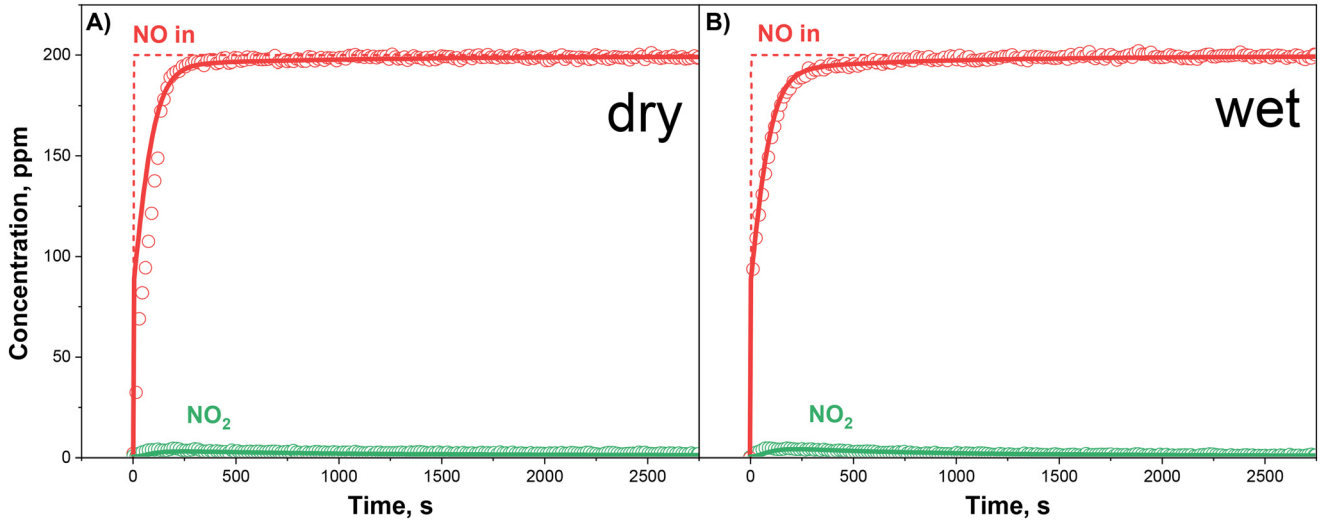

Fig. 6 NO + O_2 mixture: nominal feed concentrations (dashed lines), experimental results (dots) and kinetic simulations (solid lines) over the 0.50% Pd sample, under dry-gas (A) and wet (B) conditions. T = 100 °C, W_{cat} = 40 mg, GHSV = 300 000 $cm^3\ h^{-1}\ g_{cat}^{-1}$ (STP). Gas feed: NO = 200 ppm, CO = 0 ppm, O_2 = 10% v/v, H_2O = 0–5% v/v.

carried out at 100 °C over the 0.50% Pd sample. The results are shown here for the first time, in combination with the kinetic analysis of the adsorption step.

Fig. 6 illustrates the experiment for the NO + O_2 mixture, in the absence (Fig. 6A) and presence (Fig. 6B) of 5% v/v H_2O in the feed stream. Both experiments show the same features detected over the higher Pd-loading sample (0.84% Pd), namely an instantaneous NO adsorption upon its injection, concurrent with slow NO_2 production. Thus, the system could be described following the same reaction scheme discussed for the higher loading sample ((R4) to (R6)). Remarkably, both tests show an NO storage efficiency close to one, see Fig. 7 (0.97 and 0.95 for the dry-gas and wet mixture, respectively), in contrast to the 0.84% Pd sample where a promotion effect is observed with water.[35] This may be rationalized by the limited NO capacity to reduce Pd^{2+}, as earlier discussed. Accordingly, a lower loading may enable the reactant to completely reduce to Pd^{+} the overall palladium content even without water, while at a higher loading the effect of Pd-oxidation may become more relevant, preventing the complete reduction. Indeed, in the NO + O_2 tests, the NO storage efficiency is determined by the balance between the reductive NO adsorption steps ((R4) + (R5)), and the oxidative NO desorption step (R6), which compete with different rates at the different temperatures. This closed redox loop determines the fraction of $Pd^{+}NO$, and, thus, the amount of adsorbed NO.

It is important to assess the effect of the Pd loading on the rates of reactions (R4)–(R6) which govern the NO storage. The rate equation for the reversible adsorption of NO on $Pd^{2+}OH$ (R4) is first order in the reactive palladium species. Thus, its kinetic constants (k_4^{ads} and k_4^{des}) remain unaltered when changing the Pd loading. Instead, (R5) and (R6) (the reduction and oxidation of Pd in presence of NO) are second order in their respective palladium species (as shown in

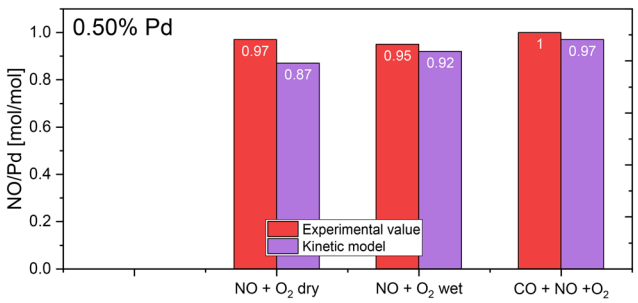

Fig. 7 Comparison between the experimental (red bars) and the kinetic model (purple bars) NO storage efficiencies with different feed gas phase compositions, over the over 0.50% Pd sample, at 100 °C.

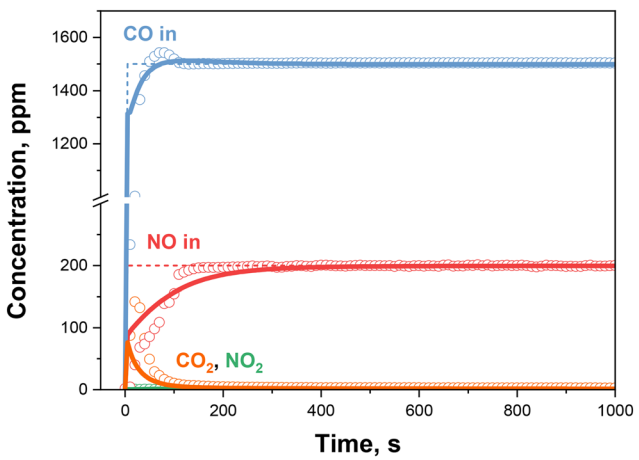

Fig. 8 CO + NO + O_2 mixture: nominal inlet concentrations (dashed lines), experimental results (dots) and kinetic simulation (solid lines) over 0.50% Pd sample. T = 100 °C, W_{cat} = 40 mg, GHSV = 300 000 $cm^3\ h^{-1}\ g_{cat}^{-1}$ (STP). Gas feed: NO = 200 ppm, CO = 1500 ppm, O_2 = 10% v/v, H_2O = 0% v/v.

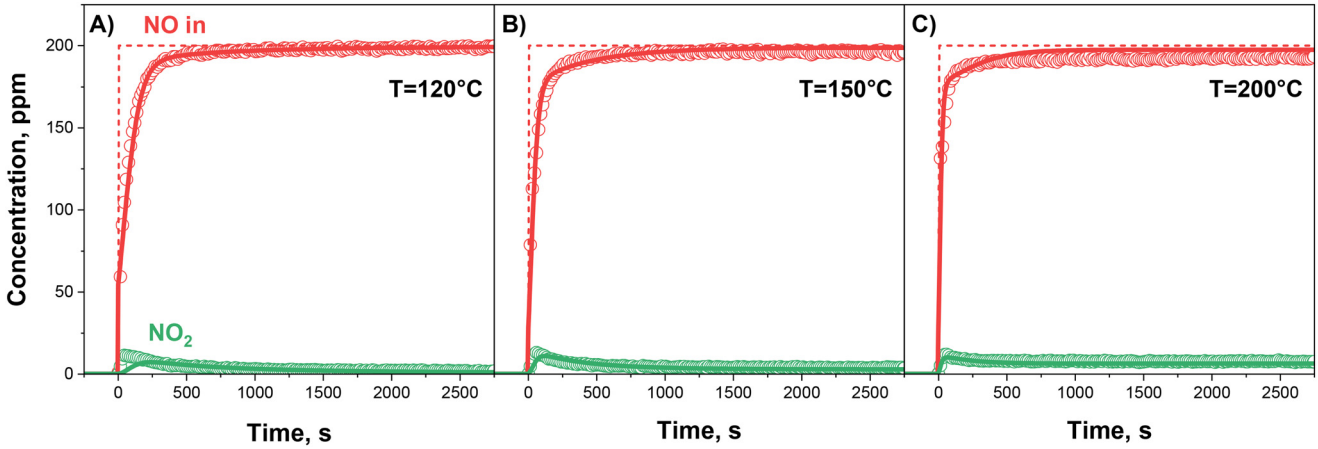

Fig. 9 NO + O_2 dry-gas mixture: nominal inlet concentrations (dashed lines), experimental results (dots) and kinetic fit (solid lines) over 0.84% Pd sample, at 120 °C (A), 150 °C (B) and 200 °C (C). T = 120/150/200 °C, W_{cat} = 40 mg, GHSV = 300 000 $cm^3\ h^{-1}\ g_{cat}^{-1}$ (STP). Gas feed: NO = 200 ppm, CO = 0 ppm, O_2 = 10% v/v, H_2O = 0% v/v.

Table 1), and their rate constants are proportional to the Pd loading. Thus, to extrapolate the kinetic constant to a different loading from the previously assessed estimates for the 0.84% Pd sample, they must be proportionally adapted as follows (n is the number of moles in the sample):

$$k(0.50\%\ \mathrm{Pd}) = \frac{n_{0.50\%\mathrm{Pd}}}{n_{0.84\%\mathrm{Pd}}} k(0.84\%\ \mathrm{Pd}) \quad (10)$$

The resulting predictive simulations (solid lines in Fig. 6) describe accurately the species temporal evolution for both feed mixtures, validating the approach for NO + O_2 systems, and the resulting integral NO storage is also close to the experimental one, as reported in Fig. 7.

Similarly, in the simultaneous presence of NO and CO, the 0.50% Pd sample resembles its higher loading counterpart (Fig. 8): a carbon dioxide production upon CO feed (R1), a CO displacement in correspondence to the NO adsorption ((R2) and (R3)), a negligible NO_2 production and the complete Pd utilization are observed, as reported in Fig. 7. The kinetic simulation, now accounting for all the reactions and using the adjusted rate constants for (R1)–(R7) is shown in Fig. 8 as solid lines. The model simulation adheres to the experimental CO profile, however, somewhat underestimating the initial CO_2 peak and predicting a slower NO adsorption rate.

Such a simplified approach in the description of the Pd-loading effect has been shown to be effective, capturing the main system features, and with a predicted NO storage efficiency close to the experimental one (0.97, Fig. 7). Furthermore, in the case of the 100 °C systems it confirms the adequacy of the Pd-redox chemistry and of the kinetic modelling methodology herein adopted, albeit further improvements may be required to enhance its accuracy.

3.3 Adsorption temperature effect

The kinetic analysis of the adsorption temperature effect (120 to 200 °C) for all the gas feed mixtures (NO + O_2 dry-gas, NO + O_2 wet, CO + O_2 + delayed NO, CO + NO + O_2) is examined over the 0.84% Pd sample in the following sections.

3.3.1 NO + O_2 dry-gas: fit at higher temperatures. Fig. 9 illustrates the transient NO and NO_2 evolution for the NO + O_2 dry-gas feed mixture upon increasing the adsorption temperature (120, 150, 200 °C). An enhanced NO adsorption rate is observed, with concurrent growing steady state value for NO_2 and decreasing value for NO; furthermore, a progressive decrement in the NO storage is found, as plotted in Fig. 10 (grey full symbols, *e.g.*, 0.77 at 120 °C, and 0.25 at 200 °C). These occurrences can be rationalized by the gradual activation of a Pd-oxidation process (R6) which limits the available adsorption sites (Pd^+), as discussed in the Material and methods.[23,35]

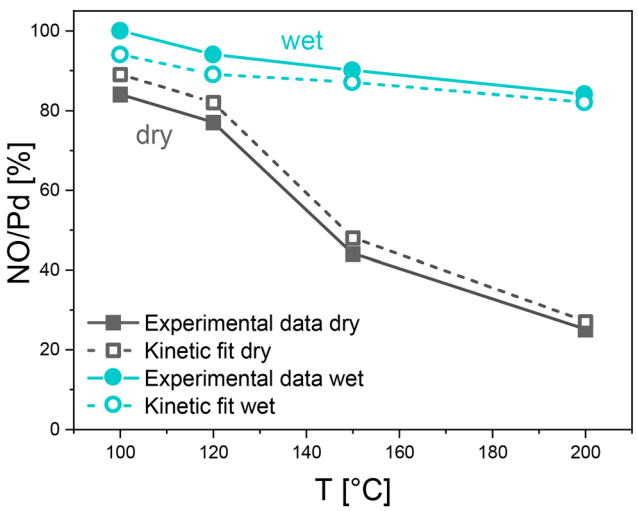

Fig. 10 Comparison between the experimental NO storage (full symbols) and the kinetic model evaluation (empty symbols), for the NO + O_2 mixture both in dry-gas (grey squares + lines) and wet (water blue circles + lines), over the 0.84% Pd sample, at different adsorption temperatures.

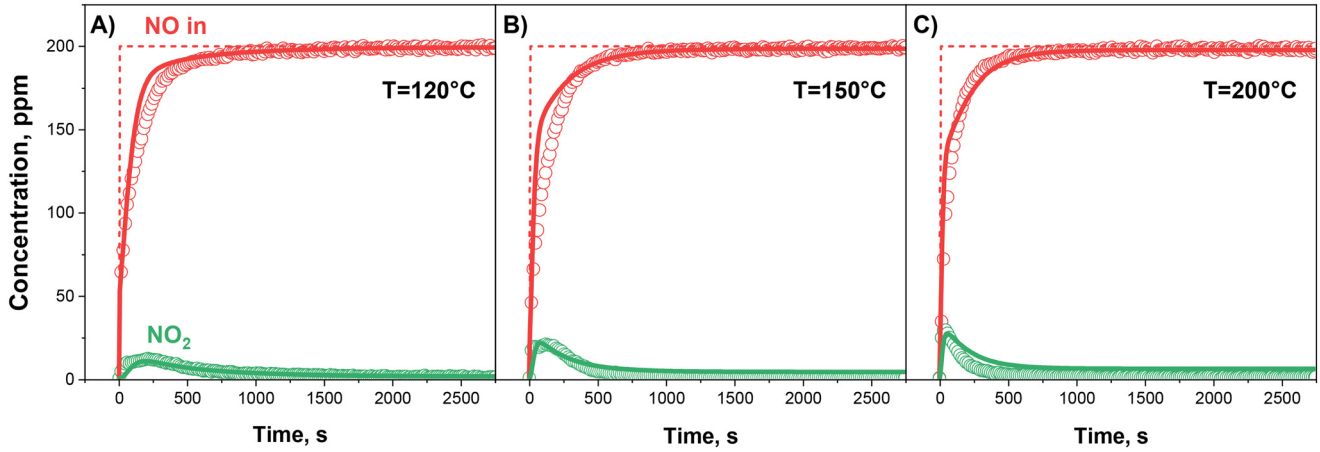

Fig. 11 NO + O_2 wet mixture: nominal inlet concentrations (dashed lines), experimental results (dots) and kinetic fit (solid lines) over the 0.84% Pd sample, at 120 °C (A), 150 °C (B) and 200 °C (C). T = 120/150/200 °C, W_{cat} = 40 mg, GHSV = 300 000 $cm^3\ h^{-1}\ g_{cat}^{-1}$ (STP). Gas feed: NO = 200 ppm, CO = 0 ppm, O_2 = 10% v/v, H_2O = 5% v/v.

The transient species concentration trends predicted by the kinetic model adhere to the experimental data, accounting for an increasing adsorption rate and a progressive change in the NO and NO_2 steady states. The monotonic decrease of the integral NO storage is also correctly traced, as documented in Fig. 10 (grey empty symbols), however with a slight overestimation with respect to the experimental data. The rate constants (k_4 to k_6) have been accordingly fitted at different temperatures ((R6) together with the TPSR fit, as seen at 100 °C), and the estimates are illustrated in terms of Arrhenius plots in Fig. SI.3.† The highest activation energy is estimated for (R6) (E_A = 69.3 kJ mol^{-1}), coherently with the proposed temperature effect where Pd-oxidation becomes progressively more relevant at higher temperatures. Nevertheless, non-negligible energy barriers have been estimated also for the other reactions.

3.3.2 NO + O_2 wet: fit of water effect. The impact of temperature in the case of the NO + O_2 wet feed mixture appears mitigated in comparison with its dry-gas counterpart. As shown by the experimental data in Fig. 11, a weaker T-effect on the steady state NO and NO_2 concentrations is observed, which remains close to the feed concentration and to zero, respectively. This is ascribed to the water inhibiting effect on the Pd-oxidation (R6), as mentioned earlier.[35] Therefore, we observe an increased availability of Pd^+ sites

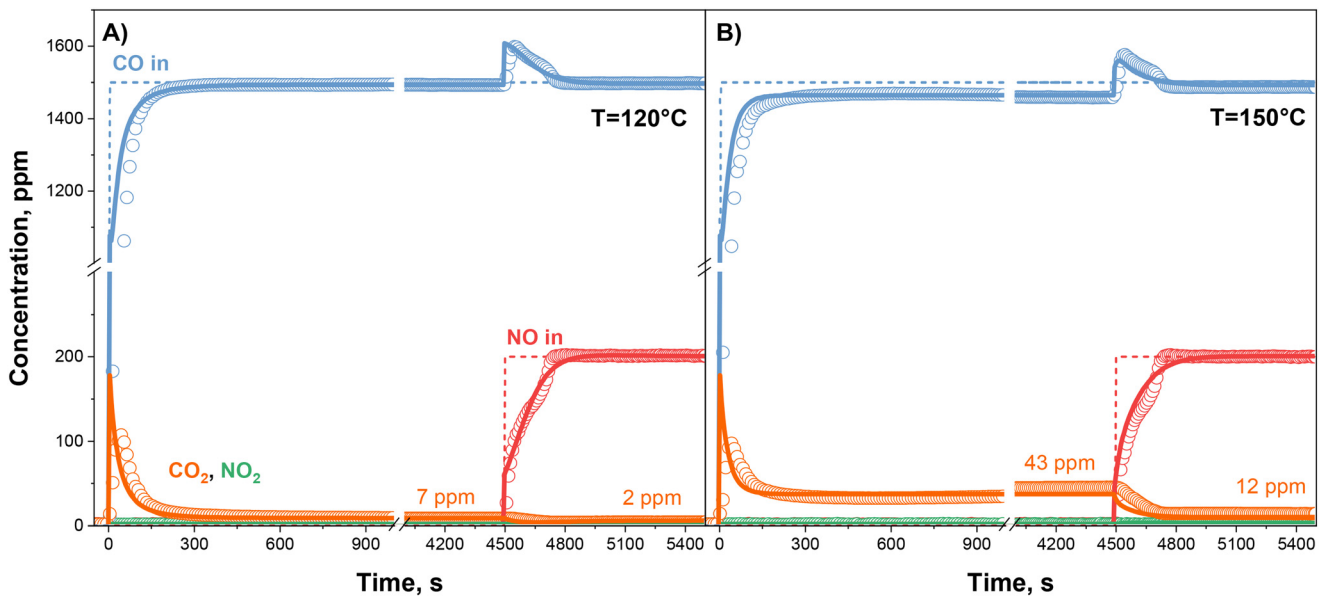

Fig. 12 CO + O_2 + delayed NO mixture: nominal inlet concentrations (dashed lines), experimental results (dots) and kinetic simulation (solid lines) over 0.84% Pd sample at 120 °C (A) and 150 °C (B). T = 120/150 °C, W_{cat} = 40 mg, GHSV = 300 000 $cm^3\ h^{-1}\ g_{cat}^{-1}$ (STP). Gas feed: CO = 1500 ppm, NO = 200 ppm, O_2 = 10% v/v, H_2O = 0% v/v.

with respect to the NO + O_2 dry-gas mixture, at the same temperature, in agreement with the high NO storage efficiencies reported in Fig. 10 (water blue full symbols). Additionally, at higher temperatures, a higher NO_2 concentration peak is visible, indicating that the reduction of $Pd^{2+}OH(NO)$ by NO is more favourable.

As to the 100 °C test, the water effect with variable adsorption temperature is simulated relying on the kinetic constants previously assessed in the absence of water; only the rate constants for (R5) and (R6) (k_5^{wet} and k_6^{wet}) are fitted to account for the water effect on the Pd-reduction/oxidation reactions. The Arrhenius plot is shown in Fig. SI.4.† An accurate match with the data is found at all temperatures for the NO and NO_2 trends (Fig. 11) and for the integral NO storage (Fig. 10).

3.3.3 CO + O_2 + delayed NO: fit at higher temperatures. To assess the *T*-dependence of (R1)–(R3) and (R7), the CO + O_2 + delayed NO experiment was replicated at 120 and 150 °C. The results for the two temperatures are shown in Fig. 12A and B, respectively. The qualitative behaviour is similar to the experiment at 100 °C (Fig. 1), showing a spike of CO_2 upon dosing CO and oxygen, while CO release and NO adsorption are observed when feeding NO. Under these conditions, NO_2 production remains undetected. Notably, a steady-state CO_2 production on the catalyst is observed, *i.e.*, 3, 7, and 43 ppm, respectively, for the tests at 100, 120, and 150 °C in the presence of solely CO and O_2. This is ascribed to the progressive activation of the Pd^+CO reoxidation reaction (R7), resulting in the operation of the full redox cycle at steady state. The CO_2 formation remains significant when NO is present, but, as observed for the test at 100 °C, the production is slightly inhibited due to site competition between NO and CO. Indeed, the CO_2 concentration at steady state with CO + O_2 + NO is 1, 2 and 12 ppm for the three experiments, respectively.

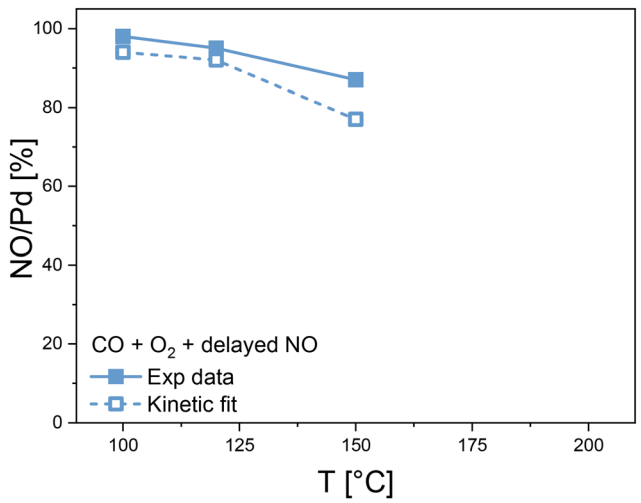

Fig. 13 Comparison between the experimental NO storage efficiency (full symbols) and the kinetic model prediction (empty symbols), for the CO + O_2 + delayed NO mixture, over the 0.84% Pd sample, at different adsorption temperatures.

The experimental results at different temperatures are compared in Fig. SI.5.† The transient profiles of CO and CO_2 are very similar at 100, 120, and 150 °C, indicating almost negligible activation energy for both the CO-mediated reduction of palladium (R1) and CO adsorption (R2). Indeed, by simulating the CO + O_2 tests with k_1 and k_2 estimated at 100 °C, the CO and CO_2 transients are well reproduced (Fig. 12, solid lines), as was the case for the test at 100 °C. For the CO release due to NO insertion (R3), the same conclusions are obtained comparing the experimental results at different temperatures, as shown in Fig. SI.6.† Indeed, the NO consumption profile does not show substantial differences at increasing temperatures. The same could be said for the CO release profile, apart from the initial and final steady states of CO due to (R7) being activated with temperature. Empirically, this means that the rate constant k_3 is not changing with temperature. The substitution of CO with NO seems then to be a non-activated reaction, at least up to 150 °C, suggesting that likely activated reactions (such as CO desorption) are not part of this competitive mechanism.

The predicted NO storage efficiency at 120 and 150 °C is consistent with the experimental trend but slightly underestimated, as shown in Fig. 13. Based on all the previous estimates of the rate constants, the steady-state production of CO_2 enables the k_7 fit at different temperatures, providing a model which can accurately predict the CO_2 value in the sole presence of CO and O_2. Furthermore, in the presence of both CO and NO, the predicted CO_2 steady-state value is again close to the experimental value, indicating the correct estimation.

When plotting the estimates of the rate constants in Arrhenius form (Fig. SI.3†), it is interesting to note that the activation energies of (R6) dry-gas and (R7) are comparable (E_A equal to 69.3 and 65.9 kJ mol^{-1}, respectively), possibly indicating similarity of the mechanisms of Pd^+ reoxidation, independently of the adsorbed species (Pd^+X, where X = CO or NO).

3.3.4 CO + NO + O_2: simulation of co-feed tests. Lastly, the system with co-feed of NO and CO is addressed at variable temperature conditions. The trend of the relevant gas phase species is illustrated in Fig. 14. In close relation to the temperature effect assessed for the CO + O_2 + delayed NO mixture, an increasing CO_2 steady state is detected, with a mirror-like decrement in the steady-state CO concentration, due to the progressive activation of Pd-oxidation (R7). However, since CO is a more effective Pd reducing agent than NO, the Pd utilization remains close to one up to 150 °C (Fig. 15), with a consistent drop only at 200 °C.[35]

An effective simulation of the gas phase trends and of the integral NO storage is achieved at all temperatures (Fig. 14), with minor deviations from the experimental features, by superimposing the rate constants assessed at 100 °C for the CO-related reactions ((R1) to (R3)) and the temperature dependent estimates for the remaining ones ((R4) to (R7)).

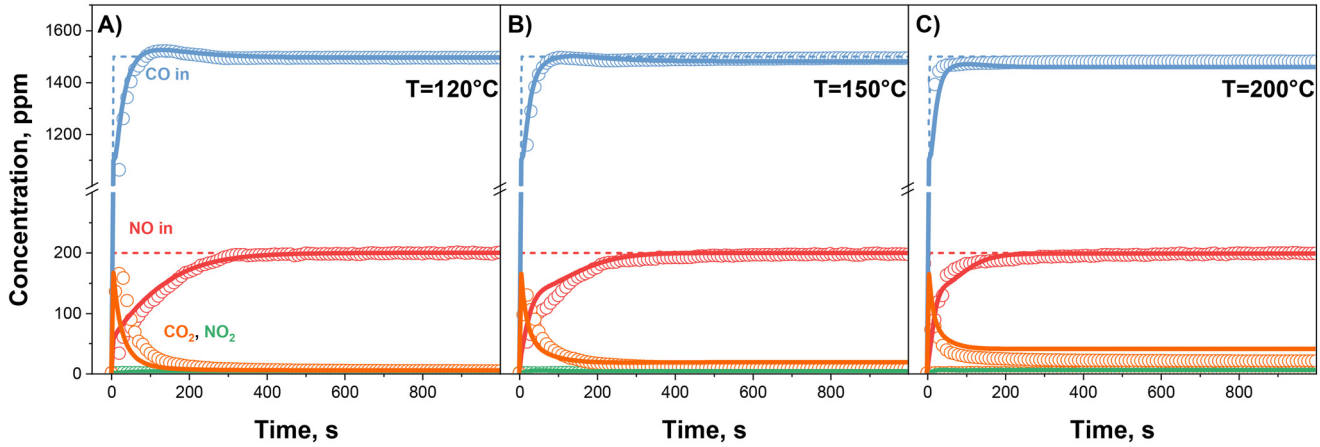

Fig. 14 CO + NO + O_2 mixture: nominal inlet concentrations (dashed lines), experimental results (dots) and kinetic simulation (solid lines) over 0.84% Pd sample at 120 °C (A), 150 °C (B) and 200 °C (C). T = 120/150/200 °C, W_{cat} = 40 mg, GHSV = 300 000 $cm^3\ h^{-1}\ g_{cat}^{-1}$ (STP). Gas feed: NO = 200 ppm, CO = 1500 ppm, O_2 = 10% v/v, H_2O = 0% v/v.

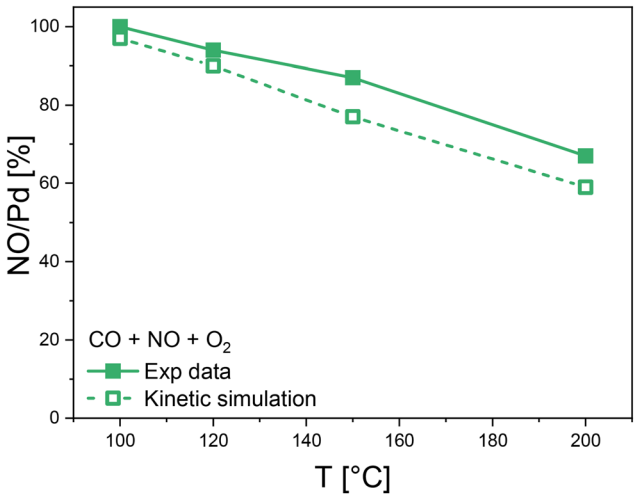

Fig. 15 Comparison between the experimental NO storage efficiency (full symbols) and the kinetic model predictions (empty symbols), for the CO + NO + O_2 mixture, over the 0.84% Pd sample, at different adsorption temperatures.

As a last step, a simple sensitivity analysis of all the kinetic parameters has been run by incrementing (3×) and decrementing (1/3×) the rate constants and comparing the related model simulations to the experimental data. Results are displayed in Fig. SI.7 of the ESI:† they indicate that the model predictions are sensitive to all the rate parameter estimates, that we can therefore regard as sufficiently robust.

4. Conclusions

This study has focused on the kinetic modelling of low-temperature NO adsorption transients over two Pd-CHA systems for PNA applications, characterized by different metal loadings (0.84% Pd and 0.50% Pd), considering different operating conditions. The goal was to gain kinetic and fundamental insight into the still debated NO adsorption chemistry.

A Pd-redox chemistry ($Pd^{2+} \leftrightarrow Pd^{+}$) previously developed has been herein considered, where CO and NO act as reducing elements for Pd^{2+} (assumed to be in the form of $Pd^{2+}OH$), while the Pd re-oxidation is ascribed to O_2, and Pd^{+} is proposed as the main NO adsorption site. A simple reacting scheme has been implemented in a transient micro-kinetic model and fitted to experiments on the two samples, with variable gas phase compositions and adsorption temperatures in the 100–200 °C range. The adopted modelling methodology focused firstly to independently assess the rate constants of two sets of reactions ((R1) to (R3) – invariant with T, (R4) to (R7) – T dependent), relying on dedicated experimental protocols (NO + O_2 dry-gas/wet, CO + O_2 + delayed NO). Then we proceeded to simulate the Pd-loading effect (0.50% Pd) on the CO + NO + O_2 systems.

A satisfactory match of the model predictions with both the observed gas phase concentration transients and the NO integral storage was found at 100 °C, thus supporting the underlying chemistry. CO, or NO, reduces $Pd^{2+}OH$ according to a dual-site mechanism, releasing CO_2, or NO_2, and so enabling the NO adsorption onto Pd^{+}. However, while CO reacts readily with $Pd^{2+}OH$, NO is less active, requiring a pre-adsorption step, forming $Pd^{2+}OH(NO)$. Notably, the fitted rate constants allowed to predict the effect of changing the Pd loading, at 100 °C, with different gas phase reactants.

Concerning the adsorption temperature effect, up to 200 °C an effective description of the NO + O_2 dry-gas system was achieved by considering the progressive activation of a Pd-oxidation process (R6): as Pd^{+} is re-oxidized, fewer NO adsorption sites remain available, which agrees closely with the observed drop of the NO storage. In the presence of water (NO + O_2 wet), the Pd^{+} reoxidation process is, however, inhibited. In addition, water promotes a higher NO_2 production peak. Thus, including account of such effects in the related steps of the model – *i.e.*, promoting reaction (R5) and inhibiting (R6) – enabled to describe successfully the NO storage at variable temperatures.

Finally, the CO + O_2 + delayed NO tests allowed to assess that reactions (R1)–(R3) are temperature independent, since the related transient profiles do not change significantly with *T*, when below 200 °C. The steady state production of CO_2 allowed to tune the *T*-dependence of the Pd^+CO oxidation (R7), which was found in close similarity to the *T*-dependence of the Pd^+NO oxidation, suggesting that there is just one Pd^+ oxidation step. Lastly, accurate simulations of the CO + NO + O_2 system were obtained by using the rate constants fitted on the independent NO + O_2 and CO + O_2 + delayed NO test runs.

The methodology based on the independent estimation of the rate constants employed in this work has therefore confirmed the validity of the proposed simple low-temperature Pd-redox chemistry for Pd-CHA PNA systems in a broad range of conditions.

Data availability

The data supporting this article are included in the main text and the ESI.† Additional data are not available.

Author contributions

Umberto Iacobone: investigation, validation, formal analysis, visualization, data curation, writing – original draft. Andrea Gjetja: investigation, validation, formal analysis, visualization, data curation, writing – original draft. Nicola Usberti: formal analysis, data curation, writing – review & editing. Isabella Nova: conceptualization, resources, supervision, writing – review & editing. Enrico Tronconi: conceptualization, resources, supervision, project administration, funding acquisition, writing – review & editing. Djamela Bounechada: conceptualization, writing – review & editing. Roberta Villamaina: investigation, conceptualization, writing – review & editing. Maria Pia Ruggeri: conceptualization, resources. Andrew P. E. York: conceptualization, writing – review & editing. Loredana Mantarosie: conceptualization. Jillian Collier: conceptualization, resources.

Conflicts of interest

There are no conflicts to declare.

Acknowledgements

This study was financially supported by Johnson Matthey.

References

1 C. K. Lambert, Perspective on SCR NO: X control for diesel vehicles, *React. Chem. Eng.*, 2019, **4**, 969–974, DOI: **10.1039/c8re00284c**.

2 A. M. Beale, F. Gao, I. Lezcano-Gonzalez, C. H. F. Peden and J. Szanyi, Recent advances in automotive catalysis for NOx emission control by small-pore microporous materials, *Chem. Soc. Rev.*, 2015, **44**, 7371–7405, DOI: **10.1039/c5cs00108k**.

3 I. Nova and E. Tronconi, *Urea-SCR Technology for deNOx After Treatment of Diesel Exhausts*, 2014, DOI: **10.1007/978-1-4899-8071-7**.

4 D. W. Fickel, E. D'Addio, J. A. Lauterbach and R. F. Lobo, The ammonia selective catalytic reduction activity of copper-exchanged small-pore zeolites, *Appl. Catal., B*, 2011, **102**, 441–448, DOI: **10.1016/j.apcatb.2010.12.022**.

5 H. Y. Chen, S. Mulla, E. Weigert, K. Camm, T. Ballinger, J. Cox and P. Blakeman, Cold Start Concept (CSC™): A Novel Catalyst for Cold Start Emission Control, *SAE Int. J. Fuels Lubr.*, 2013, **6**, 372–381, DOI: **10.4271/2013-01-0535**.

6 H. Zhao, A. J. Hill, L. Ma, A. Bhat, G. Jing and J. W. Schwank, Progress and future challenges in passive NO adsorption over Pd/zeolite catalysts, *Catal. Sci. Technol.*, 2021, **11**, 5986–6000, DOI: **10.1039/d1cy01084k**.

7 Y. Gu and W. S. Epling, Passive NOx adsorber: An overview of catalyst performance and reaction chemistry, *Appl. Catal., A*, 2019, **570**, 1–14, DOI: **10.1016/j.apcata.2018.10.036**.

8 J. Lee, J. R. Theis and E. A. Kyriakidou, Vehicle emissions trapping materials: Successes, challenges, and the path forward, *Appl. Catal., B*, 2019, **243**, 397–414, DOI: **10.1016/j.apcatb.2018.10.069**.

9 H. Y. Chen, J. E. Collier, D. Liu, L. Mantarosie, D. Durán-Martín, V. Novák, R. R. Rajaram and D. Thompsett, Low Temperature NO Storage of Zeolite Supported Pd for Low Temperature Diesel Engine Emission Control, *Catal. Lett.*, 2016, **146**, 1706–1711, DOI: **10.1007/s10562-016-1794-6**.

10 J. R. Theis and C. K. Lambert, An assessment of low temperature NOx adsorbers for cold-start NOx control on diesel engines, *Catal. Today*, 2015, **258**, 367–377, DOI: **10.1016/j.cattod.2015.01.031**.

11 O. Mihai, L. Trandafilović, T. Wentworth, F. F. Torres and L. Olsson, The Effect of Si/Al Ratio for Pd/BEA and Pd/SSZ-13 Used as Passive NOx Adsorbers, *Top. Catal.*, 2018, **61**, 2007–2020, DOI: **10.1007/s11244-018-1017-z**.

12 A. Porta, T. Pellegrinelli, L. Castoldi, R. Matarrese, S. Morandi, S. Dzwigaj and L. Lietti, Low Temperature NOx Adsorption Study on Pd-Promoted Zeolites, *Top. Catal.*, 2018, **61**, 2021–2034, DOI: **10.1007/s11244-018-1045-8**.

13 K. Khivantsev, F. Gao, L. Kovarik, Y. Wang and J. Szanyi, Molecular Level Understanding of How Oxygen and Carbon Monoxide Improve NOx Storage in Palladium/SSZ-13 Passive NOx Adsorbers: The Role of NO+ and Pd(II)(CO)(NO) Species, *J. Phys. Chem. C*, 2018, **122**, 10820–10827, DOI: **10.1021/acs.jpcc.8b01007**.

14 Y. Zheng, L. Kovarik, M. H. Engelhard, Y. Wang, Y. Wang, F. Gao and J. Szanyi, Low-Temperature Pd/Zeolite Passive NOx Adsorbers: Structure, Performance, and Adsorption Chemistry, *J. Phys. Chem. C*, 2017, **121**, 15793–15803, DOI: **10.1021/acs.jpcc.7b04312**.

15 Y. Ji, S. Bai and M. Crocker, Al2O3-based passive NOx adsorbers for low temperature applications, *Appl. Catal., B*, 2015, **170–171**, 283–292, DOI: **10.1016/j.apcatb.2015.01.025**.

16 D. Yao, P. H. Ho, R. F. Ilmasani, J. C. Wurzenberger, T. Glatz, D. Creaser and L. Olsson, Enhanced CO resistance of Pd/SSZ-13 for passive NOx adsorption, *Chem. Eng. J.*, 2023, **460**, 141681, DOI: **10.1016/j.cej.2023.141681**.

17 D. Yao, P. H. Ho, J. C. Wurzenberger, T. Glatz, W. Di, R. F. Ilmasani, D. Creaser and L. Olsson, Deciphering SO2 poisoning mechanisms for passive NOx adsorption: A kinetic modeling approach and development of a high-resistance catalyst, *Chem. Eng. J.*, 2024, **487**, 150406, DOI: **10.1016/j.cej.2024.150406**.

18 L. Castoldi, S. Morandi, P. Ticali, R. Matarrese and L. Lietti, An Assessment of Zeolite Framework Effect for Low-Temperature NOX Adsorbers, *Catalysts*, 2023, **13**, 962, DOI: **10.3390/catal13060962**.

19 A. Wang, K. Lindgren, M. Di, D. Bernin, P. A. Carlsson, M. Thuvander and L. Olsson, Insight into hydrothermal aging effect on Pd sites over Pd/LTA and Pd/SSZ-13 as PNA and CO oxidation monolith catalysts, *Appl. Catal., B*, 2020, **278**, 119315, DOI: **10.1016/j.apcatb.2020.119315**.

20 J. Lee, Y. S. Ryou, S. J. Cho, H. Lee, C. H. Kim and D. H. Kim, Investigation of the active sites and optimum Pd/Al of Pd/ZSM–5 passive NO adsorbers for the cold-start application: Evidence of isolated-Pd species obtained after a high-temperature thermal treatment, *Appl. Catal., B*, 2018, **226**, 71–82, DOI: **10.1016/j.apcatb.2017.12.031**.

21 D. Yao, R. Feizie Ilmasani, J. C. Wurzenberger, T. Glatz, J. Han, A. Wang, D. Creaser and L. Olsson, Kinetic modeling of CO assisted passive NOx adsorption on Pd/SSZ-13, *Chem. Eng. J.*, 2022, **428**, 132459, DOI: **10.1016/j.cej.2021.132459**.

22 M. Kaushik, T. S. Khan, M. A. Haider and D. Bhatia, Effect of H2O and CO on the NO Operating Cycle in Pd/CHA Passive NOx Adsorbers, *J. Phys. Chem. C*, 2024, **128**, 2814–2827, DOI: **10.1021/acs.jpcc.3c04999**.

23 M. Kaushik, G. Shrivastav, T. S. Khan, M. A. Haider and D. Bhatia, The Operating Cycle of NO Adsorption and Desorption in Pd-Chabazite for Passive NO xAdsorbers, *Langmuir*, 2021, **37**, 13799–13809, DOI: **10.1021/acs.langmuir.1c01383**.

24 K. Khivantsev, N. R. Jaegers, L. Kovarik, J. C. Hanson, F. Tao, Y. Tang, X. Zhang, I. Z. Koleva, H. A. Aleksandrov, G. N. Vayssilov, Y. Wang, F. Gao and J. Szanyi, Achieving Atomic Dispersion of Highly Loaded Transition Metals in Small-Pore Zeolite SSZ-13: High-Capacity and High-Efficiency Low-Temperature CO and Passive NOx Adsorbers, *Angew. Chem., Int. Ed.*, 2018, **57**, 16672–16677, DOI: **10.1002/anie.201809343**.

25 Y. S. Ryou, J. Lee, S. J. Cho, H. Lee, C. H. Kim and D. H. Kim, Activation of Pd/SSZ-13 catalyst by hydrothermal aging treatment in passive NO adsorption performance at low temperature for cold start application, *Appl. Catal., B*, 2017, **212**, 140–149, DOI: **10.1016/j.apcatb.2017.04.077**.

26 A. Gupta, S. B. Kang and M. P. Harold, NOx uptake and release on Pd/SSZ-13: Impact Of Feed composition and temperature, *Catal. Today*, 2021, **360**, 411–425, DOI: **10.1016/j.cattod.2020.01.018**.

27 M. Ambast, A. Gupta, B. M. M. Rahman, L. C. Grabow and M. P. Harold, NOx adsorption with CO and C2H4 on Pd/SSZ-13: Experiments and modeling, *Appl. Catal., B*, 2021, **286**, 119871, DOI: **10.1016/j.apcatb.2020.119871**.

28 P. Kim, J. Van Der Mynsbrugge, M. Head-Gordon and A. T. Bell, Experimental and Theoretical Studies of Pd Cation Reduction and Oxidation during NO Adsorption on and Desorption from Pd/H-CHA, *J. Phys. Chem. C*, 2022, **126**, 18744–18753, DOI: **10.1021/acs.jpcc.2c06357**.

29 L. Castoldi, R. Matarrese, S. Morandi, P. Ticali and L. Lietti, Low-temperature Pd/FER NOx adsorbers: Operando FT-IR spectroscopy and performance analysis, *Catal. Today*, 2021, **360**, 317–325, DOI: **10.1016/j.cattod.2020.02.019**.

30 C. Descorme, P. Gélin, M. Primet and C. Lécuyer, Infrared study of nitrogen monoxide adsorption on palladium ion-exchanged ZSM-5 catalysts, *Catal. Lett.*, 1996, **41**, 133–138, DOI: **10.1007/BF00811479**.

31 K. Mandal, Y. Gu, K. S. Westendorff, S. Li, J. A. Pihl, L. C. Grabow, W. S. Epling and C. Paolucci, Condition-Dependent Pd Speciation and NO Adsorption in Pd/Zeolites, *ACS Catal.*, 2020, **10**, 12801–12818, DOI: **10.1021/acscatal.0c03585**.

32 D. Mei, F. Gao, J. Szanyi and Y. Wang, Mechanistic insight into the passive NOx adsorption in the highly dispersed Pd/HBEA zeolite, *Appl. Catal., A*, 2019, **569**, 181–189, DOI: **10.1016/j.apcata.2018.10.037**.

33 K. Khivantsev, N. R. Jaegers, L. Kovarik, S. Prodinger, M. A. Derewinski, Y. Wang, F. Gao and J. Szanyi, Palladium/Beta zeolite passive NOx adsorbers (PNA): Clarification of PNA chemistry and the effects of CO and zeolite crystallite size on PNA performance, *Appl. Catal., A*, 2019, **569**, 141–148, DOI: **10.1016/j.apcata.2018.10.021**.

34 M. Ambast, S. A. Malamis and M. P. Harold, Coupled uptake and conversion of C12H26 and NO on Pd/SSZ-13: Experiments and modeling, *Chem. Eng. J.*, 2021, **423**, 129958, DOI: **10.1016/j.cej.2021.129958**.

35 R. Villamaina, U. Iacobone, I. Nova, E. Tronconi, M. P. Ruggeri, L. Mantarosie, J. Collier and D. Thompsett, Mechanistic insight in NO trapping on Pd/Chabazite systems for the low-temperature NOx removal from Diesel exhausts, *Appl. Catal., B*, 2021, **284**, 119724, DOI: **10.1016/j.apcatb.2020.119724**.

36 U. Iacobone, I. Nova, E. Tronconi, R. Villamaina, M. P. Ruggeri, J. Collier and D. Thompsett, Appraising Multinuclear Cu2+ Structure Formation in Cu-CHA SCR Catalysts via Low-T Dry CO Oxidation with Modulated NH3 Solvation, *ChemistryOpen*, 2022, **11**, e202200186, DOI: **10.1002/open.202200186**.

37 N. Usberti, F. Gramigni, N. D. Nasello, U. Iacobone, T. Selleri, W. Hu, S. Liu, X. Gao, I. Nova and E. Tronconi, An experimental and modelling study of the reactivity of adsorbed NH3 in the low temperature NH3-SCR reduction half-cycle over a Cu-CHA catalyst, *Appl. Catal., B*, 2020, **279**, 119397, DOI: **10.1016/j.apcatb.2020.119397**.

38 R. Matarrese, L. Castoldi, S. Morandi, P. Ticali, M. C. Valsania and L. Lietti, NO adsorption/desorption pathways over Pd/SSZ-13 low temperature NOx adsorbers investigated

by operando FT-IR spectroscopy and microreactor study, *Appl. Catal., B*, 2023, **331**, 122723, DOI: **10.1016/j.apcatb.2023.122723**.

39 U. Iacobone, I. Nova, E. Tronconi, R. Villamaina, M. P. Ruggeri, J. Collier and D. Thompsett, Transient CO Oxidation as a Versatile Technique to Investigate Cu2+ Titration, Speciation and Sites Hydrolysis on Cu–CHA Catalysts: The Cu Loading Effect, *Top. Catal.*, 2023, **66**, 761–770, DOI: **10.1007/s11244-023-01813-8**.

40 S. Morandi, L. Castoldi, R. Matarrese and L. Lietti, Novel insights on the Pd speciation in Pd/SSZ-13 and on the role of H2O in the Pd reduction by CO, *Spectrochim. Acta, Part A*, 2025, **324**, 124945, DOI: **10.1016/j.saa.2024.124945**.

41 R. Villamaina, U. Iacobone, I. Nova, M. P. Ruggeri, J. Collier, D. Thompsett and E. Tronconi, Low-T CO Oxidation over Cu −CHA Catalysts in Presence of NH 3: Probing the Mobility of Cu II Ions and the Role of Multinuclear Cu II Species, *ChemCatChem*, 2020, **12**, 3843–3848, DOI: **10.1002/cctc.202000991**.

42 U. Iacobone, W. S. Epling, I. Nova and E. Tronconi, Transient kinetic analysis of CO oxidation over a Cu-SSZ-13 catalyst proves complete conversion of ZCu2+(OH)- cations to binuclear Cu2+ species, *Chem. Eng. Sci.*, 2024, **292**, 119970, DOI: **10.1016/j.ces.2024.119970**.

43 F. Gramigni, N. D. Nasello, N. Usberti, U. Iacobone, T. Selleri, W. Hu, S. Liu, X. Gao, I. Nova and E. Tronconi, Transient Kinetic Analysis of Low-Temperature NH3-SCR over Cu-CHA Catalysts Reveals a Quadratic Dependence of Cu Reduction Rates on CuII, *ACS Catal.*, 2021, **11**, 4821–4831, DOI: **10.1021/acscatal.0c05362**.

44 N. D. Nasello, U. Iacobone, N. Usberti, A. Gjetja, I. Nova, E. Tronconi, R. Villamaina, M. P. Ruggeri, D. Bounechada, A. P. E. York and J. Collier, Investigation of Low-Temperature OHC and RHC in NH3–SCR over Cu-CHA Catalysts: Effects of H2O and SAR, *ACS Catal.*, 2024, **14**, 4265–4276, DOI: **10.1021/acscatal.4c00118**.

45 A. Hindmarsh, {ODEPACK}. A Collection of ODE System Solvers, *IMACS Transactions on Scientific Computation*, 1983, vol. 1.